Modular Coherence of Protein Dynamics in Yeast Cell Polarity

Juntao Tony Gao, Roger Guimerà, Hua Li, Inês Mendes Pinto, Marta Sales-Pardo,

Stephanie C. Wai, Boris Rubinstein* and Rong Li*

* To whom correspondence should be addressed. E-mail: RLi@stowers.org, bru@stowers.org

Supporting Online Material includes:

Supplementary Methods

Figure S1 to S9

Table S1 to S11

Movie S1 to S5

Reference 1 to 8

Supplementary Methods

Plasmid construction

The GFP-Rho1 and GFP-Rho3 integrative plasmids used for the iFRAP analysis were constructed using the pRS306 vector as a template cloned with GFP-linker-myc-Rho1 or GFP-linker-myc-Rho3 inserts under the control of the Rho1 promoter. The functionality of the GFP-Rho1 and GFP-Rho3 tagged proteins was assessed in a growth dilution assay after transformation of the pRS316-based Rho1 and Rho3 plasmids in wild type and *rho1Δ* and *rho3Δ* strains with incubation at 23°C or 37°C (Fig. S4). The pRS316 Rho1 and Rho3 plasmids were constructed by cloning the amplified Rho1 and Rho3 inserts from the respective integrative plasmids, including the Rho1 promoter, into the pRS316 vector.

Yeast Cell wall growth rate analysis

After growing overnight at 23°C, wild type and *pea2Δ* cells were washed with 1xPBS buffer and stained for 10 min with FITC-ConA (5µg/ml, Sigma). Cells were then returned to growth at 23°C for 10 min, 20 min, 30 min and 40 min respectively, washed and fixed with 5% formaldehyde at room temperature for 20min. Thereafter cells were washed and stained with Texas Red-ConA (5µg/ml, Molecular Probes) for 10 min. Cells were washed again using 1 x PBS buffer and imaged using confocal microscopy.

Identification of robust modules

Given a network, for a certain partition *P* of the nodes into modules, the modularity *M(P)* is defined as (1):

$$M \equiv \sum_{s=1}^{N_M} \left[\frac{l_s}{L} - \left(\frac{d_s}{2L} \right)^2 \right]$$

where N_M is the number of modules, L is the number of links in the network, l_s is the number of links between nodes in module s, and d_s is the sum of the connectivity (degrees) of the nodes in module s. Modules (and the optimal number of modules) are typically identified by selecting the partition P^* that maximizes $M(P)$(2). Two issues, however, make direct maximization of the modularity inappropriate for the identification of modules in protein interaction networks. First, protein interaction data reportedly contain numerous false positives and false negatives(3). Second, two different partitions of the same network can have very similar values of modularity, so that by only looking at the partition with the largest modularity some potentially relevant information is lost (4). To overcome these problems and obtain robust modules, we combine modularity maximization with an algorithm that enables one to identify both plausible missing interactions and observed interactions that are likely to be spurious (5).

Specifically, we repeat the following procedure 100 times (Fig. S2 A-D):

(i) From the observed cell polarity protein interaction network (which presumably contains errors and omissions with respect to the unknown *true* protein interaction network), we obtain a "reconstructed network" (2).

(ii) The reconstruction is built by adding plausible missing interactions and removing plausible spurious interactions, using the algorithm described in (4). In general, the reconstructed network has been shown to be closer to the true network than the observed network itself (5).

(iii) We obtain the modules in the reconstructed network by maximizing the modularity.

We obtain 100 reconstructed networks with maximal modularity value. Because of the stochasticity of the reconstruction algorithm, each reconstructed network is slightly different, and so are the modules. With the modules for each of the 100 reconstructed networks, we build a similarity matrix $\boldsymbol{S}$ whose element S_{ij} is the fraction of times which proteins *i* and *j* were placed in the same module (Fig. S2 A-D). From this matrix, we obtain the consensus modules by identifying groups of proteins that are consistently placed in the same module in the reconstructions (5) (Fig. 1A and Fig. S2 A-D).

iFRAP experiments, analysis of time-lapse movies and FRET measurements

In all iFRAP experiments, bleaching was applied on the selected area as indicated in Fig. 2 using the MicroPoint Mosaic system (Photonic Instruments, Inc., Saint Charles, IL). For proteins with $t_{1/2}$ around or longer than 60s, such as Pea2, Pkc1, and Rho1, longer image recording (4-min videos) was needed: 9 images before iFRAP bleaching, 241 images after iFRAP bleaching with time intervals of 1 s. Pulse frequency was set to 20/s and bleaching was performed for around 2 s. Time-lapse movies (2-min videos) were produced in a standardized manner for most proteins with $t_{1/2}$ less than 40 s: 31 images before photo bleaching, 241 images after photo bleaching, and time interval between every two images is 0.5 s (thus it takes less than 2.5 min to obtain one time-lapse movie). For Mkk1 which has $t_{1/2}$ less than 40 s, shorter movies were made on APD confocal microscope (ZEISS): 7 images before, and 80 images after iFRAP bleaching. For each time-lapse movie, background was subtracted and at least one control cell was used for the acquisition of photobleaching correction.

From every iFRAP time-lapse movie, log file created by Metamorph to record cellular fluorescence was uploaded into IDL 7 for background subtraction and curve analysis. Correction

from photobleaching and final curve fitting were performed using OriginPro 8 with custom-made codes. ImageJ 1.4 (http://rsb.info.nih.gov/ij) was used occasionally for visualization and quantification. For image photobleaching correction, the background-subtracted fluorescence intensity in the two control cells in every time-lapse iFRAP movie was fitted to the equation

$$Y = A\, e^{-m\, t}$$

where Y is the average fluorescence in the region of interest, A is the initial fluorescence value, and the factor $e^{-m\, t}$ was used for correction of fluorescence intensity in the bleached cell. Only curves with the photobleaching rate lower than ~10% were selected for the next step of quantification.

For iFRAP curve fitting, equation

$$Y = A_0 + A' e^{-\omega\, t}$$

was used, where $(A_0 + A')$ is the normalized initial fluorescence value and A_0 is the saturation value; and $t_{1/2} = \ln 2/\omega$. For four strains which have low GFP expression level (Gic1, Rom2, Msb4 and Mkk1), every 5 points on iFRAP curve were averaged before iFRAP curve fitting.

For the goodness-of-fit, only the curves with R-square greater than 0.3 were kept for further analysis thus leading to the average R-square value for iFRAP curves in every strain larger than 0.5. For every strain, in order to remove the outliers in $t_{1/2}$ data set, only the points which are in the range of mean ± 2 SD were kept.

For the measurement of Rho1 polarization rate in wild-type and *pea2Δ* mutant cells, sigmoid function was used to fit the Rho1 localization curve:

$$y = \frac{A_1 - A_2}{1 + e^{(x - x_0)/k}} + A_2$$

where y is a ratio of GFP-Rho1 average intensity at the polar cortex to an average intensity in the whole cell; A_1 and A_2 are the initial and final value of the ratio which can be adjusted for fitting; 1/k describes GFP-Rho1 cap formation rate at the inflection point.

The acceptor photobleaching FRET experiments and analysis were performed as described in (6). The FRET efficiency image in Fig. S7 was produced by application of the following procedure using ImageJ 1.4 software:

1. Temporal binning by 4 images (before and after photobleaching) to obtain total fluorescence F_b and F_a before and after photobleaching respectively.

2. The background was subtracted and images were spatially binned by 8 pixels.

3. For each pixel the FRET efficiency ratio F_a / F_b was calculated and the result was presented in a color heat map.

The normalized FRET efficiency ratio presented in Fig. S7 was calculated by dividing all FRET efficiency ratios of each protein interacting pair by the mean of their respective negative control, therefore setting the mean of the negative control equal to 1.

Modeling polarity protein dynamics

Consider a protein interaction network made of n functional modules. Each module is assigned the characteristic time τ_i, i = 1, 2, …, n. A protein p is characterized by the integer vector $\mathbf{N}_p = \{N_{p,1}, N_{p,2},\ldots, N_{p,n}\}$ where $N_{p,i}$ is the number of interactions of this protein with proteins from the i-th module and is determined by the network modular structure. The lifetime $T_{p,i}$ of the bond created by the protein p and the protein from the i-th module is defined as the characteristic time of the i-th module, i.e., $T_{p,i} = \tau_i$,. We estimate τ's using multivariate regression as:

$$\tau_{p,j} = \sum_{i=1}^{n} \frac{N_{p,i}}{N_p} \tau_i + e_{p,j}$$

where $\tau_{p,j}$ represents the residence time for the j-th measurement of the p^{th} protein (experimentally obtained); τ_i represents the residence time for the i^{th} module; $N_{p,i} / N_p$ represents the percentage of connections to the i^{th} module for the p^{th} protein; $N_p = \Sigma^n_{i=1} N_{p,i}$ is the total module connection for the p^{th} protein; $e_{p,j}$ is the error term.

The regression analysis was performed using SAS 9.2. We first used the data from the 29 proteins to see how well the model (Eq.2) fits the data. Then, we use a set of 10 proteins (either a chosen set or randomly drawn sets from 29 proteins without replacement, see Results), each protein having at least 10 measurements to estimate the residence time for five modules. The square root of the error mean square was recorded. This Eq.2 model was used to predict the mean residence time for those proteins not included in the training set. Pearson correlation coefficients and p-value between the predicted values and the observed mean values were calculated.

Protein dynamics and the Kuramoto model

In adapting concepts of the Kuramoto model to explain the dynamical properties of proteins in cell polarity, we consider each protein in the PCD network as a unit oscillator (oscillating between cytoplasmic and polar cortical locations) interacting with the five modular oscillators corresponding to the five sub-functions intrinsically harbored in the PCD network. Each modular oscillator is akin to a Kuramoto's "giant oscillator", however, the original theory only deals with unimodal distribution of oscillator frequencies. Pre-defining modular oscillators based on network modularity precludes the bottom up approach used in the original theory to describe the spontaneous emergence of giant oscillators as a result of oscillator coupling, but with this assumption we aimed to explore the mathematical relationship between the dynamics of

unit oscillators with the modular oscillators once the system has evolved to a steady-state, where the behavior of the "giant oscillators" is stably established (see below).

The original Kuramoto model (7) describes the phase dynamics of N>>1 identical oscillators governed by the equations $d\phi_i/dt = \omega_i+\varepsilon/N \Sigma_{j=1} \sin(\phi_j-\phi_i)$, where ε is the strength of interaction, $\phi_i(t)$ is the phase and ω_i is the natural frequency of i-th oscillator. The distribution of frequencies $g(\omega)$ is assumed to be unimodal centered around $\omega = \omega_0$. When the interaction strength ε reaches a critical value $2/(\pi g(\omega_0))$, this system of oscillators self-organizes into the "giant oscillator" characterized by a single frequency to which all unit oscillators are locked. In reference (8) it was shown that for bimodal frequency distribution, one observes emergence of two "giant oscillators" with different frequencies.

Viewing the modular structure of the PCD network as a set of five "giant oscillators", one can ask: how is the dynamics of a single unit oscillator governed by the network structure. We assume that the dynamical properties of the "giant oscillators" are not affected by their interaction with unit oscillators.

Then the phase $\phi(t)$ of the unit oscillator with a natural frequency ω is governed by the equation $d\phi/dt = \omega+\varepsilon\Sigma_{i=1} w_i \sin(\omega_i t - \phi)$, where ω_i is the i-th "giant oscillator" frequency and w_i is the weight of i-th module proportional to the number of interactions of the unit oscillator with this module ($\Sigma_{i=1} w_i = 1$). The numerical simulations of this model show that independently of the natural frequency ω value of the unit oscillator, the oscillator frequency is locked to a constant value determined by the frequencies and weights of the network modules.

One can further simplify the model by replacing the nonlinear phase interaction with a linear one, so that the governing equation reads $d\phi/dt = \omega+\varepsilon \Sigma_{i=1} w_i (\omega_i t-\phi)$. This equation admits

a stable steady state solution corresponding to the observed oscillator frequency equal to the weighted mean of the "giant oscillator" frequencies $\Sigma_{i=1}\, w_i\, \omega_i$. As we represent and measure the dynamics of proteins in the PCD by their residence times, it would be reasonable to consider a model that postulates the observed residence time τ_p of protein p (analogous to of the observed frequency of a unit oscillator) as weighted mean of the modules characteristic kinetic parameter τ_i (analogous to giant oscillator frequency ω_i) as follows $\tau_p = \Sigma_{i=1}\, w_i\, \tau_i$. The last transformation from the frequency to residence time dynamical description is not justified mathematically, but the analysis performed shows that the residence time approach describes the experimental measurements much better than the frequency-based one.

Modularity Test

To address the issue of the unimodular network structure our model predicts a single residence time t for all network components computed as simple or weighted mean of measured $t_{1/2}$. To compute the correlation between the predicted and observed values we used *Mathematica* 7.0.1 to generate 10000 sets of 29 random numbers with the average equal to t and standard deviation equal to that of the measured $t_{1/2}$. The correlation of each set with the observed values was computed and the results were averaged showing that no correlation exists, the average correlation value is 0 with the standard deviation equal to 0.07. No correlation was found greater by absolute value than 0.24.

Statistics

For the analysis comparing average $t_{1/2}$ values for two modules (Signaling and Transport), we fitted a model including module effect and protein effect such that the protein

effect was considered as nested within the module. We also fitted a model without considering the module effect to compare the difference between all proteins. Tukey method was used for pair-wise comparison. For the analysis comparing cell wall growth between wild-type and mutant cells, we fitted a two way ANOVA model including time, genotype (wild-type and mutant), and their interaction effect. For the analysis comparing the average $t_{1/2}$ values between a protein itself to its directly interacting proteins or to its indirectly interacting proteins (Table S8), we fitted a one way ANOVA model.

Supplementary Figure Legends

Fig. S1. A network of polarity protein interactions. Polarity protein network contained 99 nodes and 302 linkages obtained from BioGrid database (version 2.0.51), visualized in Cytoscape version 2.6.3.

Fig. S2. Identification of robust modules. From the observed protein interaction network (***A***), we build 100 reconstructions following Ref. (2) (***B***). For each of the reconstructed networks, we identify modules by maximizing modularity (4); therefore, we obtain 100 partitions of the nodes into modules (***C***). From the 100 partitions, we build a similarity matrix *S* whose element S_{ij} is the fraction of times which proteins *i* and *j* are in the same module (***D***). From this matrix, we obtain the consensus modules using the box identification procedure described in Ref.(5).

Fig. S3. A protein-protein similarity matrix based on the polarity protein interaction network was constructed and ordered using the network analysis scheme discussed in the text and Figure S2. Modules can be observed as distinct groups of nodes (outlined by black lines).

Fig. S4. Functional analysis of GFP-tagged Rho1 and Rho3 at different temperatures (23°C and 37°C). GFP-Rho1 and GFP-Rho3 plasmids were transformed into wild type, and the respective deletion mutant and growth analysis were performed using a 5 fold dilution drop test.

Fig. S5. A lack of correlation between $t_{1/2}$ and node properties. Scatter plots are shown of $t_{1/2}$ versus (***A***) Degree, (***B***) Betweenness, and (***C***) Participation coefficient for each protein. Additional correlation analysis results can be found in Table S7.

Fig. S6. The dynamics of two proteins in the Mitotic Exit module assessed by iFRAP. Statistical representation is the same as described in Figure 2*D* legend.

Fig. S7. FRET efficiency analysis of Pea2 and Rho1 interaction. (***A***) Pixel average FRET efficiency analysis of Pea2 and Rho1 interaction in cells expressing Pea2-mCherry and GFP-Rho1. The FRET efficiency (FE) is defined as the fluorescence intensity after photobleaching divided by the intensity before photobleaching. Scale bars: 1μm. (***B***) Analysis of FE at the bud cortex in cells expressing Pea2-mCherry and GFP-Rho1 compared with cells expressing Pea2-GFP and Spa2-mcherry (as positive control for FRET). Cells expressing Spa2-GFP or GFP-Rho1 alone were used as negative control for FRET. FE values were normalized to the respective negative control average FE.

Fig. S8. Effects of *pea2Δ* on the dynamics of 11 polarity proteins (Spa2, Bud6, Rho1, Myo2, Rho3, Lrg1, Rga1, Cdc42, Bni1, Pkc1 and Yor304c-a). The dynamics were measured as iFRAP $t_{1/2}$ and represented as in the legend of Figure 2*D* and *E* (p-value was obtained using t-test, equal variance assumed).

Fig. S9. Polarization of Rho1 in wild-type and *pea2Δ* cells. Three representative curves obtained from time-lapse imaging of cells of each genotype showing that GFP-Rho1 polarization occurred

at a significantly lower speed in wild-type cells (***A***) than in *pea2Δ* mutants (***B***). Images of a polarized wild-type (***A***) and *pea2Δ* (***B***) cell with GFP-Rho1 and kymographs of representative movies are shown next to the graphs.

Supplementary Table Legends

Table S1. List of 111 polarity proteins involved in polarity establishment and maintenance.

Table S2. 99 proteins were assigned into 5 different modules by the stochastic search algorithm mentioned in the text.

Table S3. Participation coefficient and z score to determine the role for every protein in the polarity protein network. The Participation coefficient of a node is close to 1 if its links are uniformly distributed among all modules and 0 if all of its links are within its own module. The within-module degree *z*-score measures how 'well connected' node *i* is to other nodes in the module. Z-score of 0 indicates that the number of links κ_i of node *i* to other nodes in its module s_i, is equal to the average of κ over all the nodes in module s_i.

Table S4. iFRAP $t_{1/2}$ values for the 11 GFP tagged proteins in the Signaling module.

Table S5. iFRAP $t_{1/2}$ values for the 18 GFP tagged proteins in the Transport module.

Table S6. There is no clear separation of $t_{1/2}$ values for components of Signaling and Transport modules. Pairwise comparison with Tukey multiple comparison procedure followed by one-way ANOVA was performed to test if there is significant difference in any pairwise comparisons for 29 proteins from the two modules. The proteins with the same letter show non-significant difference from each other (similar to the line plot).

Except for Pea2 and Rho1 that have large $t_{1/2}$ s, five proteins labeled with letter C (Rga1 from Signaling module, the other four from transport module) have no significant difference from each other. The majority of proteins labeled with letter D belong to either Transport or Signaling module, indicating that proteins from the same module do not always have similar $t_{1/2}$ s.

Table S7. Six commonly used parameters describing network properties and analysis of their correlation with $t_{1/2}$ values.

The six global network parameters are defined as below:

Degree: In graph theory, the degree k_i of node (vertex) *i* is the number of edges incident to the vertex, with loops counted twice. The degree is a measure of centrality since it provides a rough indication of the importance of a node based on how well it "connects".

Clustering coefficient: For node *i*, clustering coefficient is the number of pairs of neighbors of *i* that are connected divided by the total number of possible pairs of neighbors k_i (k_i -1) / 2. A clustering coefficient that is higher than that of other nodes indicates greater "cliquishness". For the whole network, one can compute the average clustering coefficient and compare it to the average coefficient expected for the equivalent random network with the same number of nodes and the same degree distribution. For the network we study, the average clustering coefficient is 0.20, which is much bigger than the one in random network.

Eccentricity: For node *i*, eccentricity is the largest distance between node *i* and any other node in the graph (provided the other node is in the same connected component). The eccentricity provides another measure of centrality since the node with the smallest eccentricity can be considered as the "closest" one to any other node in the graph.

Betweenness: For a given node, betweenness is the number of shortest paths between two nodes in a graph that go through that vertex. The betweenness is also a measure of how central a node is since the higher the betweenness of a node is, the more information flows through this node.

Once nodes are grouped into modules, each node has some connections within its own module (within module degree) and some connections to other modules. In our analysis, we use two measurements of such property:

Participation coefficient: For node *i* in module *m*, participation coefficient measures the distribution of connections among the other modules. Nodes with all the connections within their own module have a participation coefficient equal to zero whereas nodes with more connections to several other modules than to its own module have a participation coefficient that is closer to 1.

Within module degree z-score: For node *i* in module *m*, within module degree z-score measures how different the number of connections to other nodes in the same modules with respect to the distribution of within module degrees for all of the nodes in the module.

Table S8. For most of the 29 proteins that have more than one interaction partners within the PCD network, there is no predictable trend whether their dynamics are more similar to their directly interacting partners vs indirectly-interacting proteins. In this table:

Direct_mean (column B): For a given protein, **direct_mean** refers to the mean of $t_{1/2}$ values of all its direct interaction partners among the 29 proteins.

Indirect_mean (column C): For a given protein, **indirect_mean** refers to the mean of $t_{1/2}$ values of its indirect interaction partners among the 29 proteins.

Self_mean (clomun D): For a given protein, **self_mean** is the mean of $t_{1/2}$ values of this protein.

Direct p value (column E): measures the difference between **direct_mean** (column B) and **self_mean** (clomun D), that is, the difference between the mean of $t_{1/2}$ values of a given protein and the mean of $t_{1/2}$ values of this given protein's direct interaction partners. Colors indicate that there is significant difference (p value < 0.05).

Indirect p value (column F): measures the difference between **indirect_mean** (column C) and **self_mean** (clomun D), that is, the difference between the mean of $t_{1/2}$ values of the given protein and the mean of $t_{1/2}$ values of this given protein's indirect interaction partners. Colors indicate that there is significant difference (p value < 0.05).

Table S9. iFRAP $t_{1/2}$ values for the two GFP-tagged proteins (Kel1 and Lte1) in the Mitotic Exit module.

Table S10. iFRAP $t_{1/2}$ values for the effects of *pea2Δ* on the dynamics of 11 polarity proteins (Spa2, Bud6, Rho1, Myo2, Rho3, Lrg1, Rga1, Cdc42, Bni1, Pkc1 and Yor304c-a).

Table S11. Yeast strains used in this study.

Supplementary Movie Legends

Movie S1. iFRAP of GFP-Rho3. Frames were taken every 0.5 s. The cell was bleached between frame 31 and 32.

Movie S2. iFRAP of GFP-Rho1. Frames were taken every 1 s. The cell was bleached between frame 9 and 10.

Movie S3. iFRAP of Pea2-GFP. Frames were taken every 1 s. The cell was bleached between frame 9 and 10.

Movie S4. Polarization of GFP-Rho1 in a wild-type cell. Frames were taken every 60 s.

Movie S5. Polarization of GFP-Rho1 in a *pea2Δ* mutant cell. Frames were taken every 60 s.

Other iFRAP movies of GFP-tagged proteins in wild type and in mutant cells are available upon request.

Reference

1. Newman MEJ & Girvan M (2004) Finding and evaluating community structure in networks. *Phys. Rev. E* 69:no. 026113.
2. Guimerà R & Sales-Pardo M (2009) Missing and spurious interactions and the reconstruction of complex networks. (Translated from eng) *Proc. Natl Acad. Sci. USA* 106(52):22073-22078 (in eng).
3. von Mering C, *et al.* (2002) Comparative assessment of large-scale data sets of protein-protein interactions. *Nature* 417(6887):399-403.
4. Guimerà R & Amaral LAN (2005) Functional cartography of complex metabolic networks. (Translated from eng) *Nature* 433(7028):895-900 (in eng).
5. Sales-Pardo M, Guimerà R, Moreira AA, & Amaral LA (2007) Extracting the hierarchical organization of complex systems. (Translated from eng) *Proc. Natl Acad. Sci. USA* 104(39):15224-15229 (in eng).
6. Slaughter BD, Schwartz JW, & Li R (2007) Mapping dynamic protein interactions in MAP kinase signaling using live-cell fluorescence fluctuation spectroscopy and imaging. *Proc. Natl Acad. Sci. USA* 104(51):20320-20325.
7. Kuramoto Y (1984) *Chemical Oscillations, Waves, and Turbulence* (Dover Publications).
8. Strogatz SH (2000) From Kuramoto to Crawford: Exploring the onset of synchronization in populations of coupled oscillators. *Physica D* 143:1-20.

Supplementary Figure 1

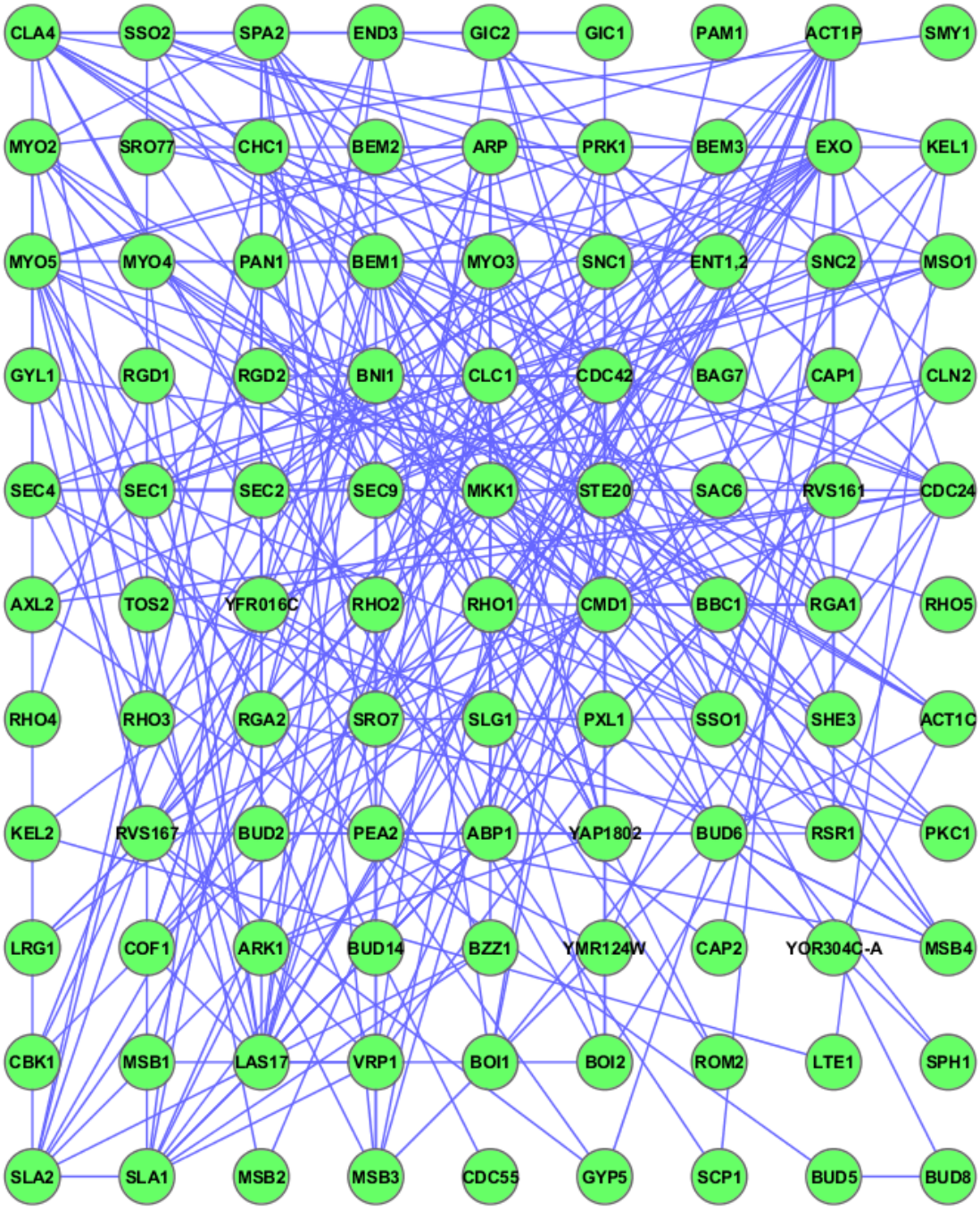

Supplementary Figure 2

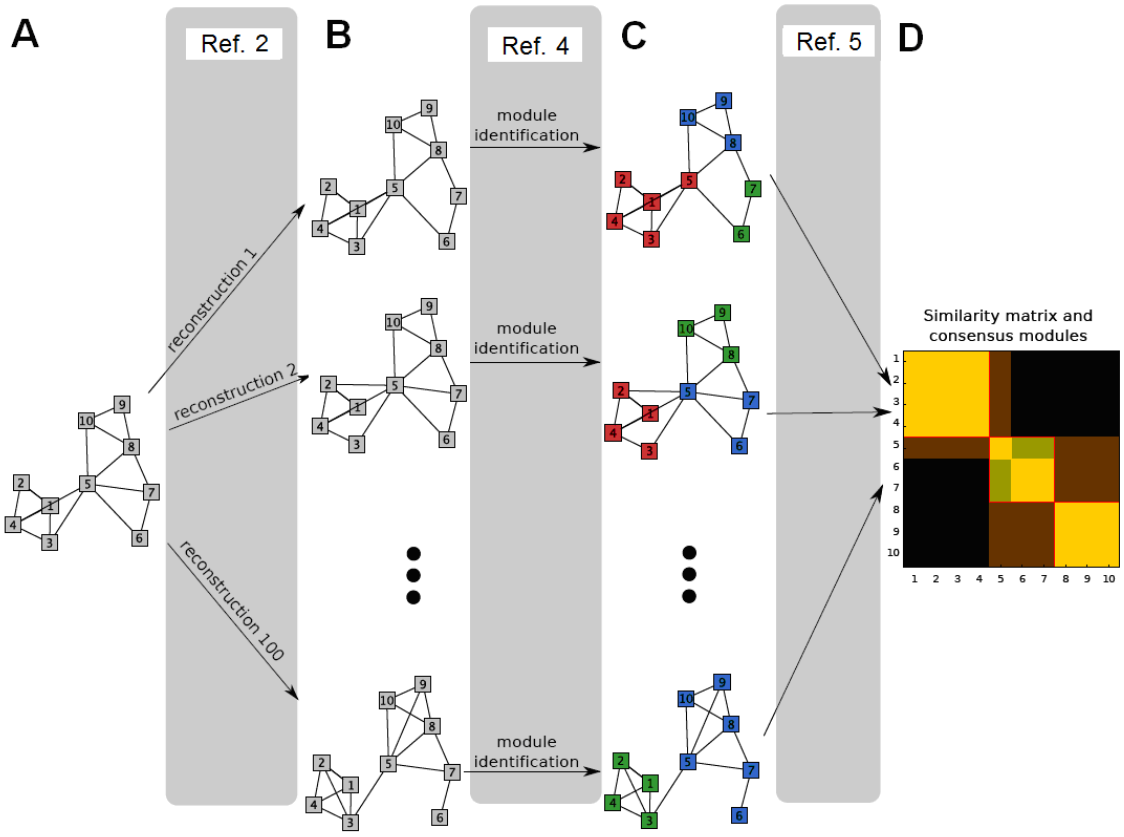

Supplementary Figure 3

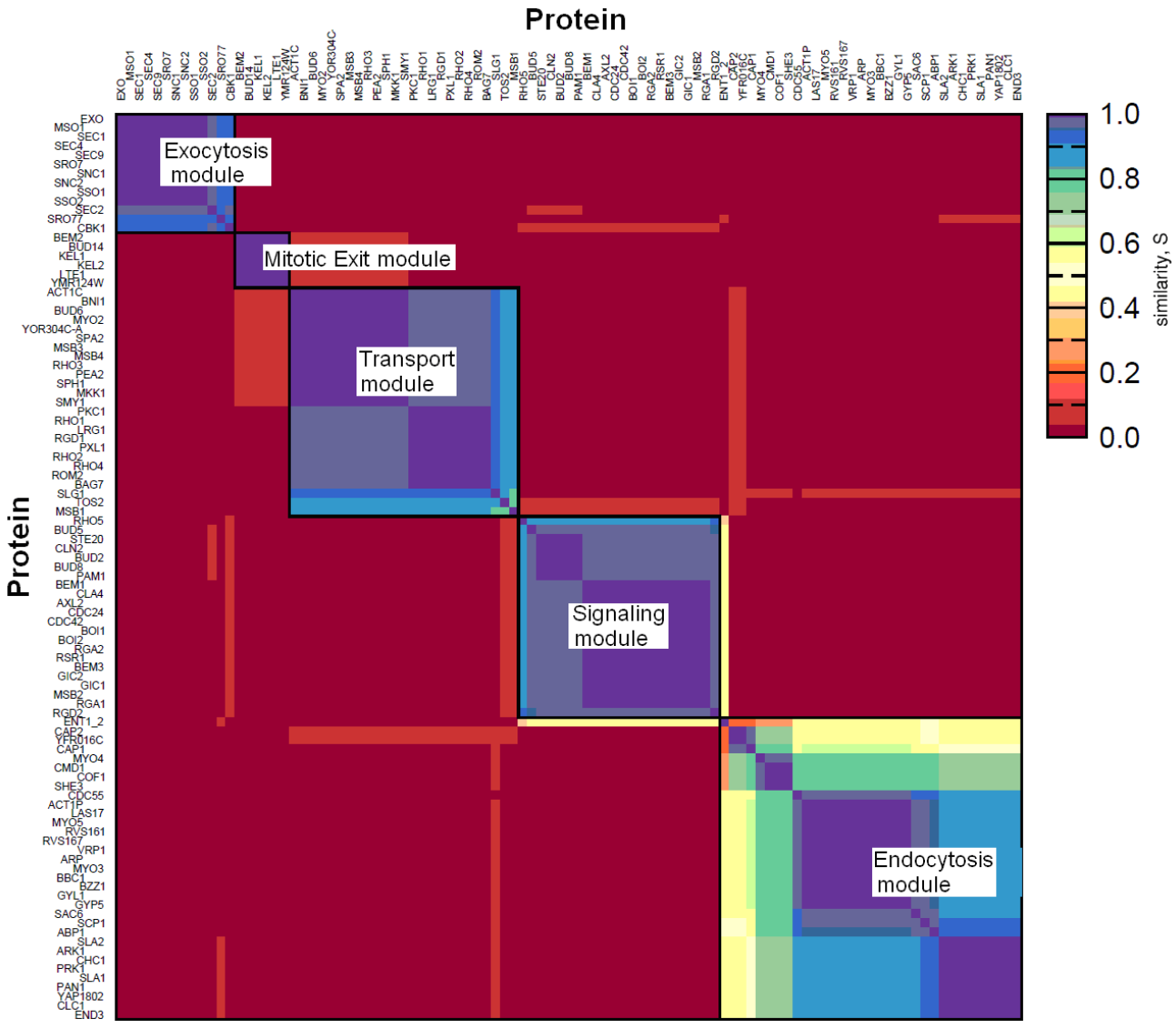

Supplementary Figure 4

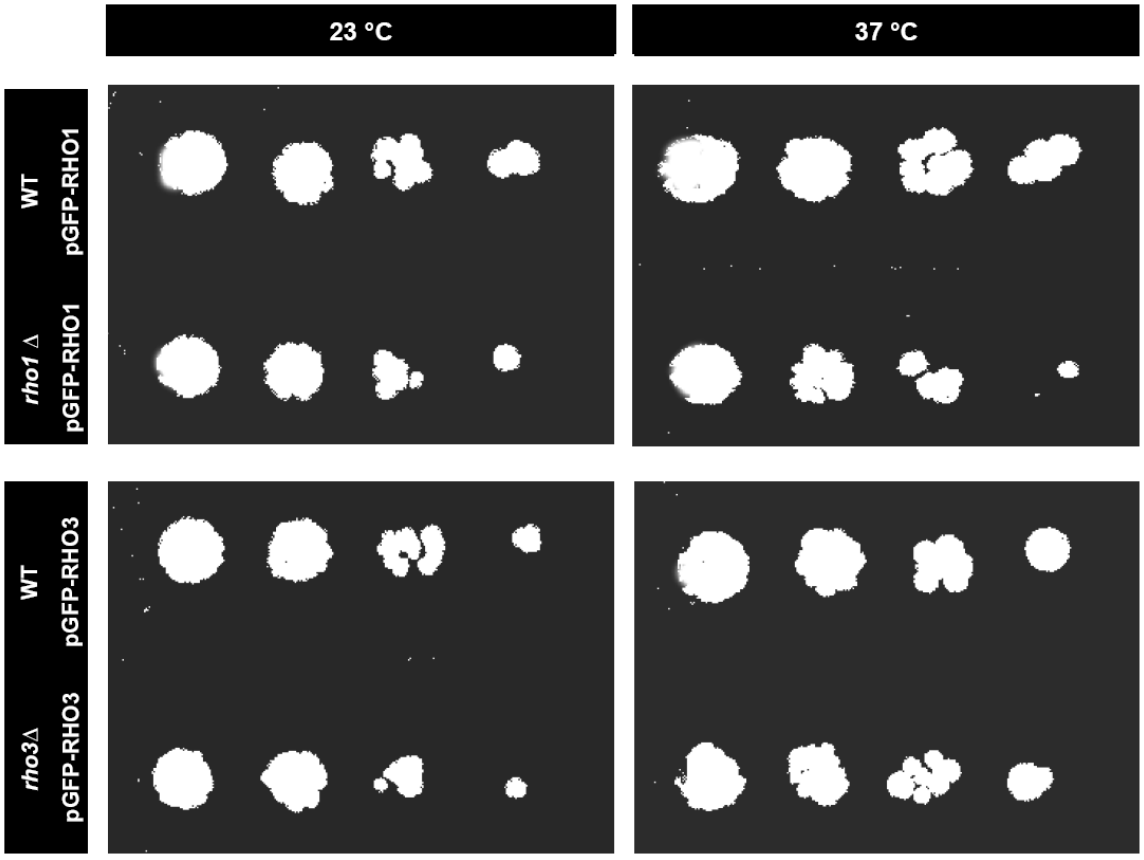

Supplementary Figure 5

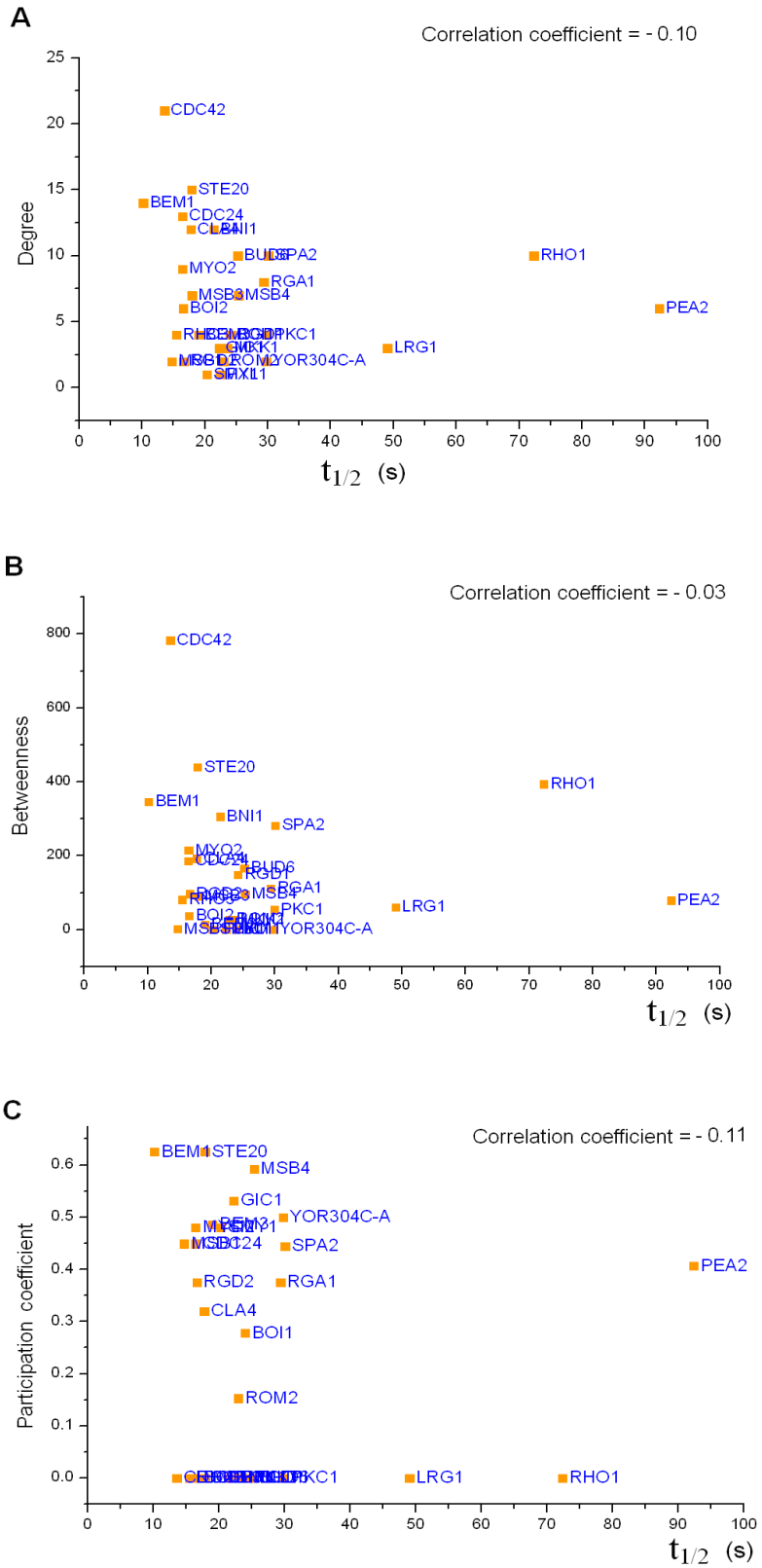

Supplementary Figure 6

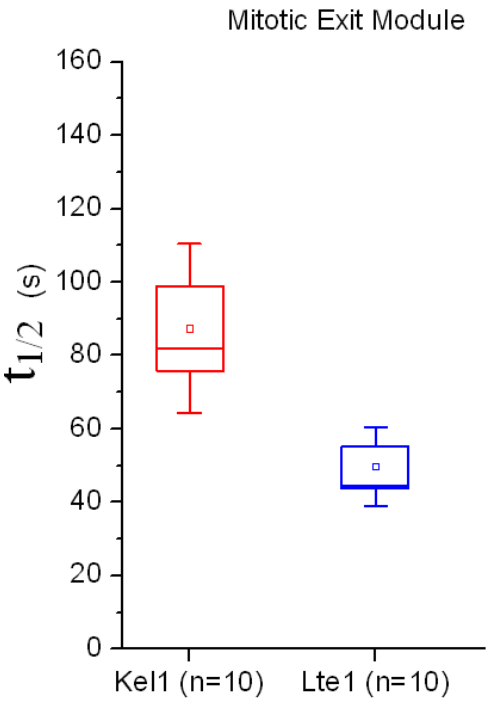

Supplementary Figure 7

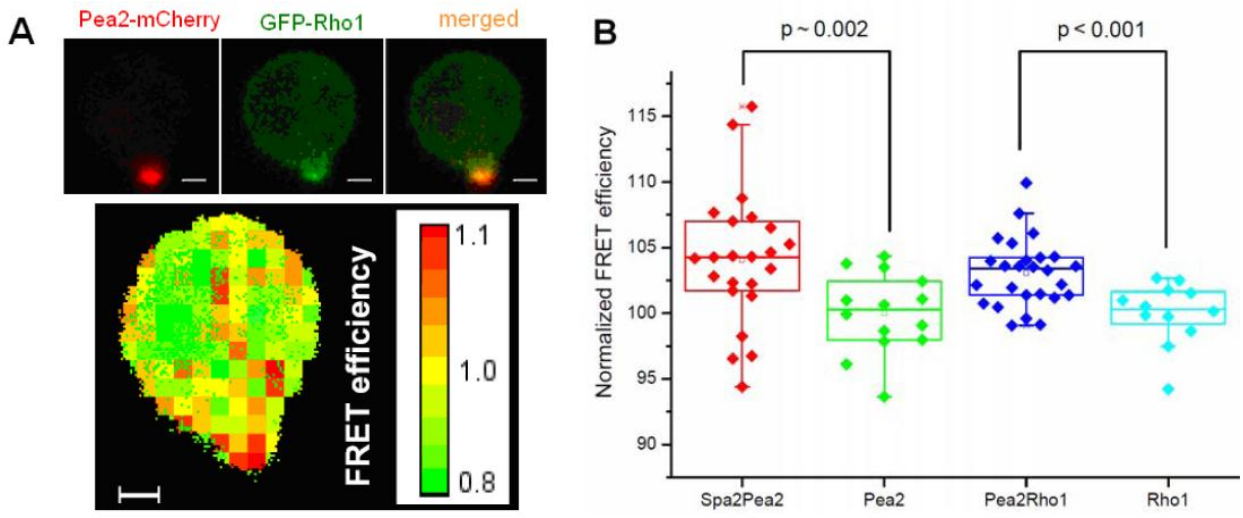

Supplementary Figure 8

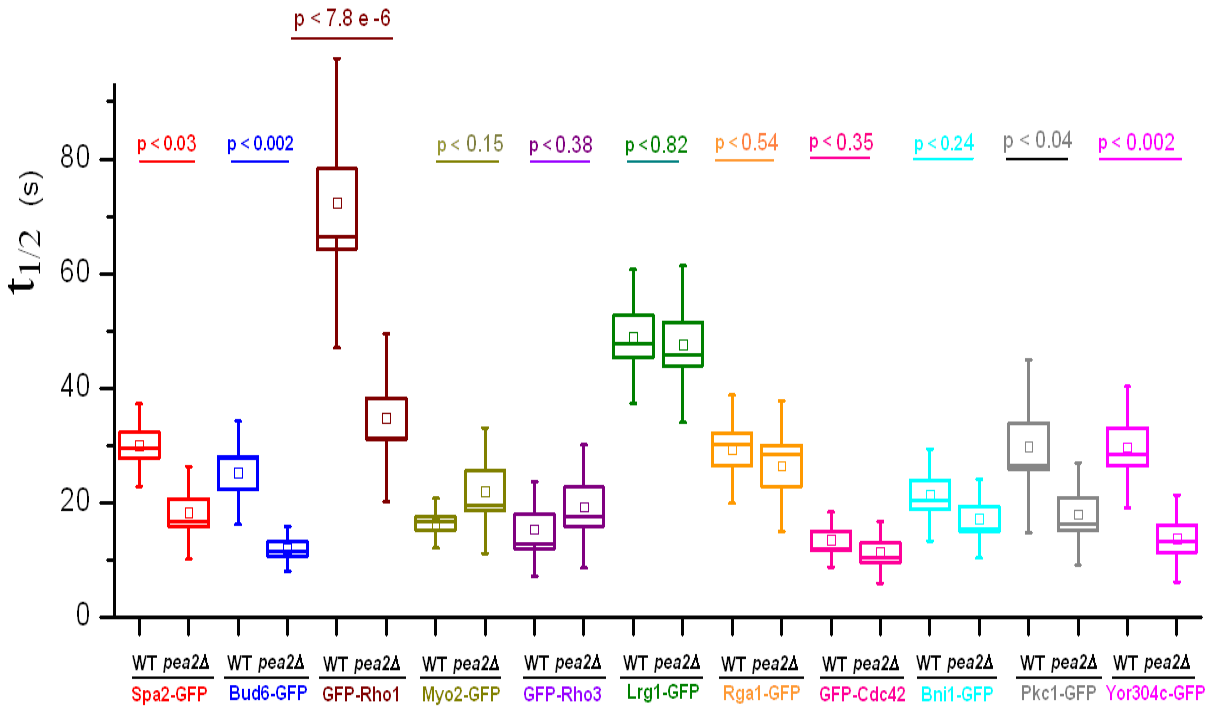

Supplementary Figure 9

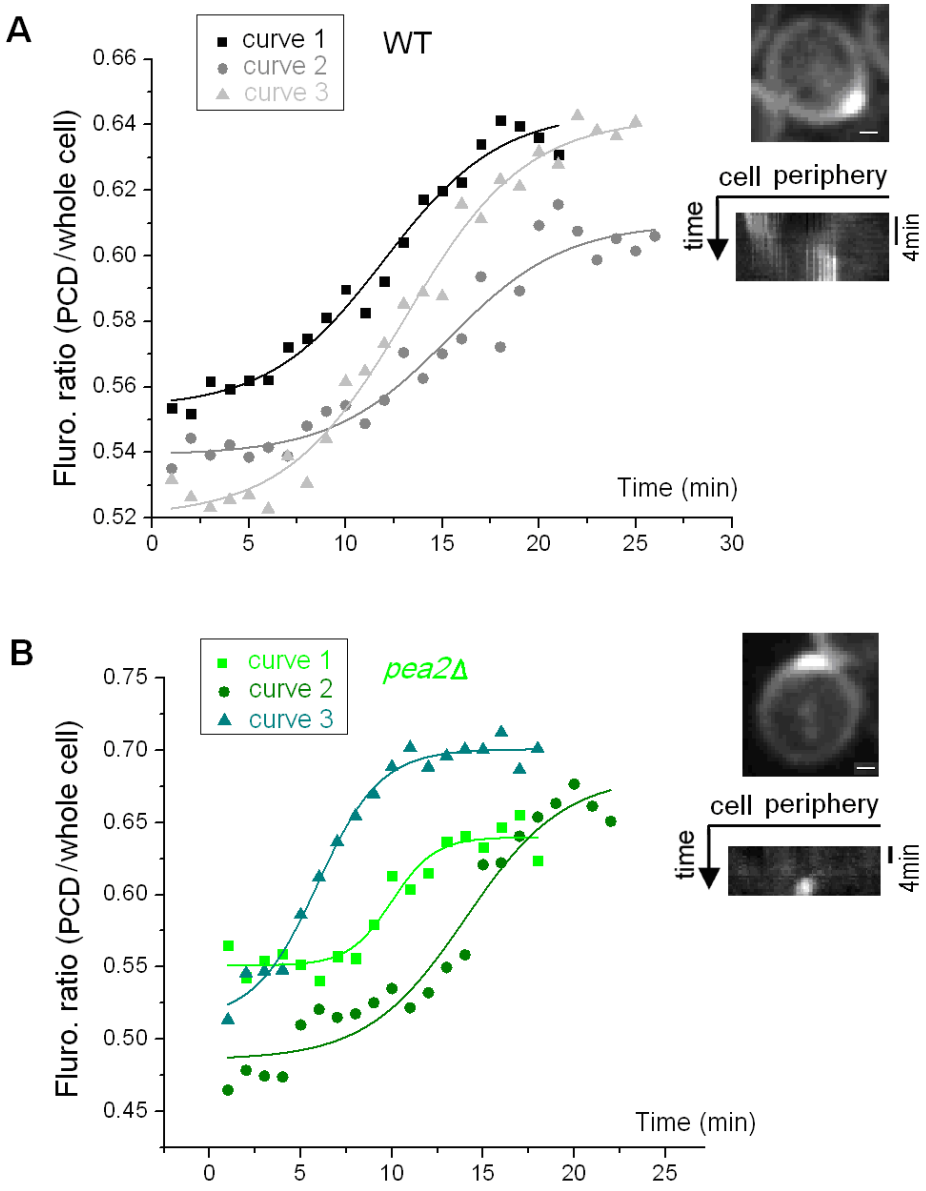

Table S1. 111 Proteins in the yeast PCD area

ORF	protein name (as appears in BioGRID)	function description	localization
YCR088W	**ABP1**	Actin-binding protein of the cortical actin cytoskeleton, important for activation of the Arp2/3 complex that plays a key role actin in cytoskeleton organization	bud
YEL039C	**ACT1C**	Actin, structural protein involved in cell polarization, endocytosis, and other cytoskeletal functions	contractile ring (sensu Saccharomyces)
YFL039C	**ACT1P**	Actin, structural protein involved in cell polarization, endocytosis, and other cytoskeletal functions	contractile ring (sensu Saccharomyces)
YNL020C	**ARK1**	Serine/threonine protein kinase involved in regulation of the cortical actin cytoskeleton; involved in control of endocytosis	bud
	ARP	Arp2/3 complex is a highly conserved actin nucleation center required for the motility and integrity of actin patches; involved in endocytosis and membrane growth and polarity	bud
YIL140W	**AXL2**	Integral plasma membrane protein required for axial budding in haploid cells; localizes to the incipient bud site and bud neck	bud neck
YOR154W	**BAG7**	Rho GTPase activating protein (RhoGAP), stimulates the intrinsic GTPase activity of Rho1p, which plays a role in actin cytoskeleton organization and control of cell wall synthesis; structurally and functionally related to Sac7p	bud
YJL020C	**BBC1**	Protein possibly involved in assembly of actin patches; interacts with an actin assembly factor Las17p and with the SH3 domains of Type I myosins Myo3p and Myo5p; localized predominantly to cortical actin patches	bud
YBR200W	**BEM1**	Protein containing SH3-domains, involved in establishing cell polarity and morphogenesis	bud tip, bud neck
YER155C	**BEM2**	Rho GTPase activating protein (RhoGAP) involved in the control of cytoskeleton organization and cellular morphogenesis; required for bud emergence	bud
YPL115C	**BEM3**	Rho GTPase activating protein (RhoGAP) involved in control of the cytoskeleton organization; targets the essential Rho-GTPase Cdc42p, which controls establishment and maintenance of cell polarity, including bud-site assembly	bud
YNL271C	**BNI1**	Formin, nucleates the formation of linear actin filaments, involved in cell processes such as budding and mitotic spindle orientation which require the formation of polarized actin cables, functionally redundant with BNR1	bud tip, bud neck
YBL085W	**BOI1**	Protein implicated in polar growth, functionally redundant with Boi2p	bud, bud neck
YER114C	**BOI2**	Protein implicated in polar growth, functionally redundant with Boi1p	bud, bud neck
YAR014C	**BUD14**	Protein involved in bud-site selection	bud tip, bud neck
YKL092C	**BUD2**	GTPase activating factor for Rer1p/Bud1p required for both axial and bipolar budding patterns; mutants exhibit random budding in all cell types	bud
YCR038C	**BUD5**	GTP/GDP exchange factor for Rer1p (Bud1p) required for both axial and bipolar budding patterns	bud neck
YLR313C	**BUD6**	Actin- and formin-interacting protein, involved in actin cable nucleation and polarized cell growth; isolated as bipolar budding mutant; potential Cdc28p substrate	bud
YLR353W	**BUD8**	Protein involved in bud-site selection	bud tip
YHR114W	**BZZ1**	SH3 domain protein implicated in the regulation of actin polymerization, able to recruit actin polymerization machinery through its SH3 domains, colocalizes with cortical actin patches and Las17p, interacts with type I myosins	bud
YNL278W	**CAF120**	Part of the evolutionarily-conserved CCR4-NOT transcriptional regulatory complex involved in controlling mRNA initiation, elongation, and degradation	bud
YKL007W	**CAP1**	Alpha subunit of the capping protein (CP) heterodimer (Cap1p and Cap2p) which binds to the barbed ends of actin filaments preventing further polymerization; localized predominantly to cortical actin patches	bud
YIL034C	**CAP2**	Beta subunit of the capping protein (CP) heterodimer (Cap1p and Cap2p) which binds to the barbed ends of actin filaments preventing further polymerization; localized predominantly to cortical actin patches	bud
YNL161W	**CBK1**	Serine/threonine protein kinase that regulates cell morphogenesis pathways	bud, bud neck
YAL041W	**CDC24**	Guanine nucleotide exchange factor (GEF or GDP-release factor) for Cdc42p	bud neck
YLR229C	**CDC42**	Small rho-like GTPase, essential for establishment and maintenance of cell polarity	bud tip, bud neck
YGL190C	**CDC55**	Non-essential regulatory subunit B of protein phosphatase 2A	bud tip, bud neck
YGL030C	**CHC1**	Clathrin heavy chain, subunit of the major coat protein involved in intracellular protein transport and endocytosis; two heavy chains form the clathrin triskelion structural component; the light chain (CLC1) is thought to regulate function	bud
YJL158C	**CIS3**	Mannose-containing glycoprotein constituent of the cell wall	bud tip
YNL298W	**CLA4**	Cdc42p-activated signal transducing kinase of the PAK (p21-activated kinase) family, which also includes Ste20p and Skm1p; involved in septin ring assembly, vacuole inheritance, and cytokinesis; phosphorylates septins Cdc3p and Cdc10p	bud
YGR167W	**CLC1**	Clathrin light chain, subunit of the major coat protein involved in intracellular protein transport and endocytosis; thought to regulate clathrin function; two Clathrin heavy chains (CHC1) form the clathrin triskelion structural component	bud
YPL256C	**CLN2**	G1 cyclin involved in regulation of the cell cycle; activates Cdc28p kinase to promote the G1 to S phase transition; late G1 specific expression depends on transcription factor complexes, MBF (Swi6p-Mbp1p) and SBF (Swi6p-Swi4p)	bud
YBR160C	**CMD1**	Calmodulin	bud tip, bud neck
YLL050C	**COF1**	Cofilin, promotes actin filament depolarization in a pH-dependent manner; binds both actin monomers and filaments and severs filaments; thought to be regulated by phosphorylation at SER4; ubiquitous and essential in eukaryotes	bud
YCR017C	**CWH43**	Putative sensor/transporter protein involved in cell wall biogenesis	bud tip, bud neck
YGR168W	**DNF1**	Aminophospholipid translocase (flippase) that localizes primarily to the plasma membrane; contributes to endocytosis, protein transport and cell polarity; type 4 P-type ATPase	bud
YNL084C	**END3**	EH domain-containing protein involved in endocytosis, actin cytoskeletal organization and cell wall morphogenesis; forms a complex with Sla1p and Pan1p	bud
	ENT1,2	Epsin-like protein involved in endocytosis and actin patch assembly and functionally redundant with End2p; binds clathrin via a clathrin-binding domain motif at C-terminus	bud
	EXO	Essential protein with dual roles in spliceosome assembly and exocytosis	bud tip, bud neck
YHR061C	**GIC1**	Protein of unknown function involved in initiation of budding and cellular polarization, interacts with Cdc42p via the Cdc42/Rac-interactive binding (CRIB) domain	bud tip, bud neck
YDR309C	**GIC2**	Protein of unknown function involved in initiation of budding and cellular polarization, interacts with Cdc42p via the Cdc42/Rac-interactive binding (CRIB) domain	bud tip
YMR192W	**GYL1**	Putative GTPase activating protein (GAP) that may have a role in polarized exocytosis	bud, bud tip, bud neck
YPL249C	**GYP5**	GTPase-activating protein (GAP) for yeast Rab family members, involved in ER to Golgi trafficking	bud tip, bud neck
YMR183C	**INP2**	Peroxisome-specific receptor important for peroxisome inheritance; co-fractionates with peroxisome membranes and co-localizes with peroxisomes in vivo; physically interacts with the myosin V motor Myo2p; INP2 is not an essential gene	bud
YHR158C	**KEL1**	Protein required for proper cell fusion and cell morphology	bud tip, bud neck
YGR238C	**KEL2**	Protein that functions in a complex with Kel1p to negatively regulate mitotic exit; interacts with Tem1p and Lte1p	bud tip, bud neck
YCR161W	**LAS17**	Actin assembly factor, activates the Arp2/3 protein complex that nucleates branched actin filaments; localizes with the Arp2/3 complex to actin patches; homolog of the human Wiskott-Aldrich syndrome protein (WASP)	bud
YDL240W	**LRG1**	Putative GTPase-activating protein (GAP) involved in the Pkc1p-mediated signaling pathway that controls cell wall integrity	bud neck
YAL024C	**LTE1**	Putative GDP/GTP exchange factor required for mitotic exit at low temperatures	bud
YOR231W	**MKK1**	Mitogen-activated kinase kinase involved in protein kinase C signaling pathway that controls cell integrity	bud tip
YOR188W	**MSB1**	Protein involved in positive regulation of both 1,3-beta-glucan synthesis and the Pkc1p-MAPK pathway, potential Cdc28p substrate	bud tip, bud neck
YGR014W	**MSB2**	Mucin family member involved in the Cdc42p- and MAP kinase-dependent filamentous growth signaling pathway; also functions as an osmosensor in parallel to the Sho1p-mediated pathway; potential Cdc28p substrate	bud
YNL293W	**MSB3**	GTPase-activating protein for Sec4p and several other Rab GTPases, regulates exocytosis via its action on Sec4p, also required for proper actin organization	bud tip
YCL112W	**MSB4**	GTPase-activating protein of the Ras superfamily that acts primarily on Sec4p, localizes to the bud site and bud tip, has similarity to Msb2p	bud tip
YNR046C	**MSC1**	Probable component of the secretory vesicle docking complex, acts at a late step in secretion; shows genetic and physical interactions with Sec1p; required for prospore membrane formation during sporulation	bud
YOR326W	**MYO2**	One of two type V myosin motors (along with MYO4) involved in actin-based transport of cargos; required for the polarized delivery of secretory vesicles, the vacuole, late Golgi elements, peroxisomes, and the mitotic spindle	bud
YKL129C	**MYO3**	One of two type I myosins; localizes to actin cortical patches; deletion of MYO3 has little effect on growth, but myo3 myo5 double deletion causes severe defects in growth and actin cytoskeleton organization	bud
YAL029C	**MYO4**	One of two type V myosin motors (along with MYO2) involved in actin-based transport of cargos; required for mRNA transport, including ASH1 mRNA, and facilitating the growth and movement of ER tubules into the growing bud along with She3p	bud
YMR109W	**MYO5**	One of two type I myosins; contains proline-rich tail homology 2 (TH2) and SH3 domains; MYO5 deletion has little effect on growth, but myo3 myo5 double deletion causes severe defects in growth and actin cytoskeleton organization	bud
YDR351W	**PAM1**	Essential protein of unknown function	bud, bud neck
YIR008C	**PAN1**	Part of actin cytoskeleton-regulatory complex Pan1p-Sla1p-End3p, associates with actin patches on the cell cortex; promotes protein-protein interactions essential for endocytosis; previously thought to be a subunit of poly(A) ribonuclease	bud
YER149C	**PEA2**	Coiled-coil polarisome protein required for polarized morphogenesis, cell fusion, and low-affinity Ca2+ influx; forms polarisome complex with Bni1p, Bud6p, and Spa2p; localizes to sites of polarized growth	bud
YBL105C	**PKC1**	Protein serine/threonine kinase essential for cell wall remodeling during growth; localized to sites of polarized growth and the mother-daughter bud neck; homolog of the alpha, beta, and gamma isoforms of mammalian protein kinase C (PKC)	bud
YIL095W	**PRK1**	Protein serine/threonine kinase; regulates the organization and function of the actin cytoskeleton through the phosphorylation of the Pan1p-Sla1p-End3p protein complex	bud
YKR092W	**PXL1**	LIM domain-containing protein that localizes to sites of polarized growth, required for selection and/or maintenance of polarized growth sites, may modulate signaling by the GTPases Cdc42p and Rho1p	bud, bud tip, bud neck
YGR127W	**RGA1**	GTPase-activating protein for the polarity-establishment protein Cdc42p; implicated in control of septin organization, pheromone response, and haploid invasive growth	bud
YDR379W	**RGA2**	GTPase-activating protein for the polarity-establishment protein Cdc42p; implicated in control of septin organization, pheromone response, and haploid invasive growth; regulated by Phs8p and Cdc28p	bud
YBR260C	**RGD1**	GTPase-activating protein (RhoGAP) for Rho3p and Rho4p, possibly involved in control of actin cytoskeleton organization	bud
YFL047W	**RGD2**	GTPase-activating protein (RhoGAP) for Cdc42p and Rho5p	bud neck
YPR165W	**RHO3**	GTP-binding protein of the rho subfamily of Ras-like proteins, involved in establishment of cell polarity	bud tip, bud neck
YNL090W	**RHO2**	Non-essential small GTPase of the Rho/Rac subfamily of Ras-like proteins, involved in the establishment of cell polarity and in microtubule assembly	bud
YIL118W	**RHO3**	Non-essential small GTPase of the Rho/Rac subfamily of Ras-like proteins involved in the establishment of cell polarity; GTPase activity positively regulated by the GTPase activating protein (GAP) Rga1p	bud
YKR055W	**RHO4**	Non-essential small GTPase of the Rho/Rac subfamily of Ras-like proteins, likely to be involved in the establishment of cell polarity	bud
YNL098C	**RHO5**	Non-essential small GTPase of the Rho/Rac subfamily of Ras-like proteins, likely involved in protein kinase C (Pkc1p)-dependent signal transduction pathway that controls cell integrity	bud
YGR070W	**ROM1**	GDP/GTP exchange protein (GEP) for Rho1p; mutations are synthetically lethal with mutations in rom2, which also encodes a GEP	bud
YLR371W	**ROM2**	GDP/GTP exchange protein (GEP) for Rho1p and Rho2p	bud tip
YGR152C	**RSR1**	GTP-binding protein of the ras superfamily required for bud site selection, morphological changes in response to mating pheromone, and efficient cell fusion	bud neck
YCR009C	**RVS161**	Amphiphysin-like lipid raft protein; interacts with Rvs167p and regulates polarization of the actin cytoskeleton, endocytosis, cell polarity, cell fusion and viability following starvation or osmotic stress	bud
YDR388W	**RVS167**	Actin-associated protein, interacts with Rvs161p to regulate actin cytoskeleton, endocytosis, and viability following starvation or osmotic stress; homolog of mammalian amphiphysin	bud
YDR129C	**SAC6**	Fimbrin, actin-bundling protein; cooperates with Scp1p (calponin/transgelin) in the organization and maintenance of the actin cytoskeleton	bud
YOR367W	**SCP1**	Component of cortical actin cytoskeleton, binds and cross links actin filaments; originally identified by its homology to calponin (contains a calponin-like repeat) but the Scp1p domain structure is more similar to transgelin	bud
YDR164C	**SEC1**	Sm-like protein involved in docking and fusion of exocytic vesicles through binding to assembled SNARE complexes at the membrane	bud tip, bud neck
YNL272C	**SEC2**	Guanyl-nucleotide exchange factor for the small G-protein Sec4p; essential for post-Golgi vesicle transport; associates with the exocyst, via exocyst subunit Sec15p, on secretory vesicles	bud
YFL005W	**SEC4**	Secretory vesicle-associated Rab GTPase essential for exocytosis; associates with the exocyst component Sec15p and may regulate polarized delivery of transport vesicles to the exocyst at the plasma membrane	bud
YGR009C	**SEC9**	t-SNARE protein important for fusion of secretory vesicles with the plasma membrane; similar to but not functionally redundant with Spo20p; SNAP-25 homolog	bud
YBR130C	**SHE3**	Protein that acts as an adaptor between Myo4p and the She2p-mRNA complex; part of the mRNA localization machinery that restricts accumulation of certain proteins to the bud; also required for cortical ER inheritance	bud
YKR100C	**SKG1**	Transmembrane protein of unknown function	bud, bud tip
YLR187W	**SKG3**	Protein of unknown function	bud, bud neck
YHR149C	**SKG6**	Integral membrane protein that localizes primarily to growing sites such as the bud tip or the cell periphery; potential Cdc28p substrate; Skg6p interacts with Zds1p and Zds2p	bud
YBL007C	**SLA1**	Cytoskeletal protein binding protein required for assembly of the cortical actin cytoskeleton; interacts with proteins regulating actin dynamics and proteins required for endocytosis; found in the nucleus and cell cortex; has 3 SH3 domains	bud
YNL243W	**SLA2**	Transmembrane actin-binding protein involved in membrane cytoskeleton assembly and cell polarization; adaptor protein that links actin to clathrin and endocytosis; present in the actin cortical patch of the emerging bud tip; dimer in vivo	bud
YOR086C	**SLG1**	Sensor-transducer of the stress-activated PKC1-MPK1 kinase pathway involved in maintenance of cell wall integrity; involved in organization of the actin cytoskeleton; secretory pathway Wsc1p is required for the arrest of secretion response	bud tip, bud neck
YKL079W	**SMY1**	Protein that interacts with Myo2p, proposed to be involved in exocytosis	bud
YAL030W	**SNC1**	Vesicle membrane receptor protein (v-SNARE) involved in the fusion between Golgi-derived secretory vesicles with the plasma membrane; proposed to be involved in endocytosis; member of the synaptobrevin/VAMP family of R-type v-SNARE proteins	bud
YOR327C	**SNC2**	Vesicle membrane receptor protein (v-SNARE) involved in the fusion between Golgi-derived secretory vesicles with the plasma membrane; member of the synaptobrevin/VAMP family of R-type v-SNARE proteins	bud tip, bud neck
YLL023W	**SPA2**	Component of the polarisome, which functions in actin cytoskeletal organization during polarized growth	bud tip, bud neck
YLR313C	**SPH1**	Protein involved in shmoo formation and bipolar bud site selection	bud
YPR032W	**SRO7**	Effector of Rab GTPase Sec4p, forms a complex with Sec4p and t-SNARE Sec9p; involved in exocytosis and docking and fusion of post-Golgi vesicles with plasma membrane; homolog of Sro77p and Drosophila lgl tumor suppressor	bud
YBL106C	**SRO77**	Protein with roles in exocytosis and calcium homeostasis; functions in docking and fusion of post-Golgi vesicles with plasma membrane; homolog of Sro7p and Drosophila lethal giant larvae tumor suppressor; interacts with SNARE protein Sec9p	bud
YPL232W	**SSO1**	Plasma membrane t-SNARE involved in fusion of secretory vesicles at the plasma membrane and in vesicle fusion during sporulation; forms a complex with Sec9p that binds v-SNARE Snc2p; syntaxin homolog; functionally redundant with Sso2p	bud
YMR183C	**SSO2**	Plasma membrane t-SNARE involved in fusion of secretory vesicles at the plasma membrane; syntaxin homolog that is functionally redundant with Sso1p	bud
YHL007C	**STE20**	Cdc42p-activated signal transducing kinase of the PAK (p21-activated kinase) family, involved in pheromone response, pseudohyphal/invasive growth, and vacuole inheritance; GBB motif (found in noncatalytic domains of PAKs) binds Ste4p	bud, bud neck
YPL032C	**SVL3**	Protein of unknown function, mutant phenotype suggests a potential role in vacuolar function	bud
YGR221C	**TOS2**	Protein involved in localization of Cdc3p to the site of bud growth; may act as a membrane anchor; localizes to the bud neck and bud tip; potentially phosphorylated by Cdc28p	bud
YLR357C	**VRP1**	Proline-rich actin-associated protein involved in cytoskeletal organization and cytokinesis; related to mammalian Wiskott-Aldrich syndrome protein (WASP)-interacting protein (WIP)	bud
YAP1802	**YAP1802**	Protein involved in clathrin cage assembly; binds Pan1p and clathrin; homologous to Yap1801p, member of the AP180 protein family	bud
YPR016C	**YPR016C**	Putative protein of unknown function; green fluorescent protein (GFP)-fusion protein localizes to the cytoplasm and bud; interacts with Spa2p; YFL016C is not an essential gene	bud
YLR414C	**YLR414C**	Putative protein of unknown function; localizes to bud and cytoplasm; co-localizes with Sur7p in punctate patches in the plasma membrane; null mutant displays decreased thermotolerance; transcription induced on cell wall damage	bud
YMR124W	**YMR124W**	Protein of unknown function; green fluorescent protein (GFP)-fusion protein localizes to the cell periphery, cytoplasm, bud, and bud neck; interacts with Cmr1p in two-hybrid assay; YMR124W is not an essential gene	bud, bud neck
YMR295C	**YMR295C**	Protein of unknown function that associates with ribosomes; green fluorescent protein (GFP)-fusion protein localizes to the cell periphery and bud; YMR295C is not an essential gene	
YOR304C-A	**YOR304C-A**	Protein of unknown function; green fluorescent protein (GFP)-fusion protein localizes to the cell periphery, cytoplasm, bud, and bud neck	

Note:

In this paper,

ACT1 is divided into two groups, according to its localization and function: **ACT1C** (actin cables), localized at the actin cable; and **ACT1P** (Actin patches), localized to the actin patch.

ARP2 and ARP3 are included in the same complex called **ARP**.

Homologous proteins ENT1 and ENT2 are included in the same complex called **ENT1,2** .

SEC3, SEC5, SEC6, SEC8, SEC10, SEC15, EXO70, EXO84 are included in the same complex called **EXO**.

All proteins names in this table are in upper case. This is to keep consistent with the protein names in Biogrid database.

Table S2. Five modules in budding yeast polarity protein interaction network

Module name	Mitotic Exit	Endocytosis	Transport	Signaling	Exocytosis
Node number in a module	6	33	25	22	13
	Bem2	Abp1	Act1C	Axl2	Cbk1
	Bud14	Act1P	Bag7	Bem1	Exo
	Kel1	Ark1	Bni1	Bem3	Mso1
	Kel2	Arp	Bud6	Boi1	Sec1
	Lte1	Bbc1	Lrg1	Boi2	Sec2
	Ymr124w	Bzz1	Mkk1	Bud2	Sec4
		Cap1	Msb1	Bud5	Sec9
		Cap2	Msb3	Bud8	Snc1
		Cdc55	Msb4	Cdc24	Snc2
		Chc1	Myo2	Cdc42	Sro7
		Clc1	Pea2	Cla4	Sro77
		Cmd1	Pkc1	Cln2	Sso1
		Cof1	Pxl1	Gic1	Sso2
		End3	Rgd1	Gic2	
		Ent1,2	Rho1	Msb2	
		Gyl1	Rho2	Pam1	
		Gyp5	Rho3	Rga1	
		Las17	Rho4	Rga2	
		Myo3	Rom2	Rgd2	
		Myo4	Slg1	Rho5	
		Myo5	Smy1	Rsr1	
		Pan1	Spa2	Ste20	
		Prk1	Sph1		
		Rvs161	Tos2		
		Rvs167	Yor304c-a		
		Sac6			
		Scp1			
		She3			
		Sla1			
		Sla2			
		Vrp1			
		Yap1802			
		Yfr016c			

Table S3. Participation coefficient and z-score for 99 proteins

	Participation coefficient	z-score
ABP1	0.17	1.06
ACT1C	0.34	1.63
ACT1P	0.50	0.3
ARK1	0.28	-0.36
ARP	0.37	0.2
AXL2	0.00	-0.28
BAG7	0.00	-0.98
BBC1	0.32	-0.64
BEM1	0.54	1.19
BEM2	0.63	-0.26
BEM3	0.00	-0.28
BNI1	0.49	2.03
BOI1	0.00	-0.28
BOI2	0.28	0.01
BUD14	0.00	-0.26
BUD2	0.00	-0.87
BUD5	0.00	-0.87
BUD6	0.18	2.46
BUD8	0.00	-0.87
BZZ1	0.00	-0.64
CAP1	0.64	0
CAP2	0.00	0
CBK1	0.67	-1.98
CDC24	0.27	1.78
CDC42	0.45	2.95
CDC55	0.00	-1.5
CHC1	0.28	-0.36
CLA4	0.38	1.19
CLC1	0.32	-0.64
CLN2	0.32	-0.28
CMD1	0.48	0.2
COF1	0.56	-0.93
END3	0.32	-0.64
ENT1,2	0.58	-0.28
EXO	0.70	0.55
GIC1	0.00	-0.57
GIC2	0.53	0.01
GYL1	0.00	-0.93
GYP5	0.00	-0.93
KEL1	0.28	2.13
KEL2	0.00	-0.26
LAS17	0.28	2.77
LRG1	0.44	-0.55
LTE1	0.00	-0.26
MKK1	0.00	-0.12
MSB1	0.50	-0.98
MSB2	0.00	-0.87
MSB3	0.45	0.74
MSB4	0.57	0.3
MSO1	0.00	0.97
MYO2	0.59	0.74
MYO3	0.40	0.77
MYO4	0.48	-0.93
MYO5	0.15	1.34
PAM1	0.00	-1.16
PAN1	0.31	0.77
PEA2	0.50	0.3
PKC1	0.38	-0.12
PRK1	0.41	-0.07
PXL1	0.00	-0.98
RGA1	0.41	0.3
RGA2	0.00	0.01
RGD1	0.38	-0.12
RGD2	0.00	-0.87
RHO1	0.46	1.6
RHO2	0.00	-0.55
RHO3	0.38	-0.12
RHO4	0.00	-0.98
RHO5	0.00	-1.16
ROM2	0.00	-0.55
RSR1	0.24	0.3
RVS161	0.00	-0.07
RVS167	0.15	1.34
SAC6	0.00	-1.22
SCP1	0.00	-1.22
SEC1	0.00	0.97
SEC2	0.63	-0.71
SEC4	0.47	-0.29
SEC9	0.00	1.82
SHE3	0.32	-0.64
SLA1	0.17	1.06
SLA2	0.20	0.49
SLG1	0.50	-0.98
SMY1	0.00	-0.98
SNC1	0.00	0.13
SNC2	0.00	-0.29
SPA2	0.48	1.6
SPH1	0.00	-0.55
SRO7	0.45	-0.29
SRO77	0.44	-1.56
SSO1	0.00	0.55
SSO2	0.00	0.13
STE20	0.62	0.89
TOS2	0.50	-0.98
VRP1	0.00	0.2
YAP1802	0.00	-0.07
YFR016C	0.63	0
YMR124W	0.50	-1.06
YOR304C-A	0.00	-0.55

Table S4 . $t_{1/2}$ values for proteins in Signaling module

(equation $Y = A0 + A^* \exp(-\omega * t)$ was used for iFRAP curve fitting, for details see supplementary online material.)

	Bem1	Bem3	Boi1	Boi2	Cdc24	Cdc42	Cla4	Gic1	Rga1	Rgd2	Ste20
curve 1	4.32	21.34	21.89	25.22	13.31	10.44	13.94	16.82	30.11	11.74	9.00
curve 2	19.08	23.08	27.13	29.81	8.08	17.75	10.67	26.11	18.99	21.20	30.83
curve 3	9.22	14.04	22.01	8.86	24.80	19.91	14.92	27.74	33.10	15.70	19.61
curve 4	5.62	21.38	15.34	14.94	15.17	14.71	17.89	17.85	26.19	14.02	10.92
curve 5	15.74	10.24	26.41	6.68	17.40	7.86	18.36	15.05	42.90	16.68	15.32
curve 6	15.92	16.52	30.35	9.25	24.11	12.61	8.91	19.70	17.07	23.06	22.48
curve 7	8.75	27.77	23.75	7.98	14.44	21.92	21.34	21.87	41.14	18.08	14.44
curve 8	14.13	14.23	28.84	19.28	11.57	8.98	20.56	20.16	28.59	18.29	14.28
curve 9	8.37	18.94	18.61	11.83	14.31	10.49	30.60	36.56	39.15	21.59	18.40
curve 10	4.58	22.52	21.61	31.31	20.60	10.86	25.32	20.20	15.45	12.17	23.20
curve 11	5.98		27.85		10.49		12.57		30.32	9.93	
curve 12					16.48						
curve 13					28.24						
curve 14					10.72						

Table S5 . $t_{1/2}$ values for proteins in Transport module
(equation $Y = A0 + A^* \exp(-\omega * t)$ was used for iFRAP curve fitting, for details see supplementary online material.)

	Bni1	Bud6	Lrg1	Msb1	Msb3	Myo2	Pea2	Pkc1	Pxl1
curve 1	20.37	26.57	52.87	18.73	15.44	17.47	41.73	49.18	29.07
curve 2	15.42	14.11	44.18	14.67	13.00	12.36	79.33	48.27	15.83
curve 3	33.07	18.26	60.98	20.32	24.47	19.85	65.38	45.79	33.36
curve 4	29.75	29.14	30.29	5.60	8.35	24.45	143.99	57.63	18.73
curve 5	26.81	30.14	49.84	10.68	15.18	17.79	64.72	13.91	13.74
curve 6	14.36	30.19	38.97	11.31	13.00	19.00	148.54	12.84	18.20
curve 7	18.79	13.82	61.24	14.70	22.29	17.37	121.05	11.64	15.53
curve 8	27.87	16.13	38.75	8.08	20.13	16.75	133.65	20.17	32.28
curve 9	6.93	34.91	45.76	14.12	22.50	13.01	69.65	29.07	29.37
curve 10	20.39	39.10	67.18	28.74	27.03	11.57	54.91	26.87	17.98
curve 11					10.77	16.12		16.32	
curve 12					23.06	11.67		26.12	
curve 13						23.70		25.04	
curve 14						16.14		35.58	
curve 15						9.22			

	Rgd1	Rho1	Rho3	Smy1	Spa2	Yor304c-a	Mkk1	Msb4	Rom2
curve 1	33.70	91.15	26.37	12.01	25.04	18.36	23.30	14.15	16.22
curve 2	26.45	101.67	24.18	14.41	19.42	28.85	18.00	45.78	32.52
curve 3	33.06	101.73	12.83	12.94	28.76	28.20	22.96	38.90	16.85
curve 4	21.89	123.08	6.99	17.43	31.85	18.12	35.25	20.00	17.18
curve 5	26.32	56.96	11.24	20.87	28.99	16.27	18.99	16.01	38.54
curve 6	38.75	52.51	4.89	34.66	30.25	33.70	13.26	16.83	26.03
curve 7	15.95	95.08	23.43	14.03	42.95	27.23	31.61	16.39	21.71
curve 8	10.98	45.28	24.11	24.83	31.61	39.75	28.09	25.79	13.32
curve 9	14.62	46.51	10.17	23.26	22.18	48.74	26.28	16.68	28.83
curve 10	20.14	39.87	10.09	28.25	39.58	38.13	17.54	42.71	17.94
curve 11		72.65							
curve 12		57.36							
curve 13		94.75							
curve 14		94.65							
curve 15		60.81							
curve 16		58.28							
curve 17		67.88							
curve 18		41.14							

Table S6. There is no clear separation of $t_{1/2}$ values between two modules

module	protein	LSMean	Line2	Line1
column A	column B	column C	column D	column E
transport	Pea2	92.2958	A	
transport	Rho1	72.2976	B	
transport	Lrg1	49.0053	C	
transport	Spa2	30.0618	C	D
transport	Pkc1	29.8887	C	D
transport	Yor304c-a	29.7346	C	D
signaling	Rga1	29.3638	C	D
transport	Msb4	25.3230		D
transport	Bud6	25.2383		D
transport	Rgd1	24.1865		D
signaling	Boi1	23.9802		D
transport	Mkk1	23.5280		D
transport	Rom2	22.9140		D
transport	Pxl1	22.4097		D
signaling	Gic1	22.2062		D
transport	Bni1	21.3748		D
transport	Smy1	20.2712		D
signaling	Bem3	19.0057		D
transport	Msb3	17.9355		D
signaling	Ste20	17.8486		D
signaling	Cla4	17.7356		D
signaling	Rgd2	16.5862		D
signaling	Boi2	16.5163		D
transport	Myo2	16.4315		D
signaling	Cdc24	16.4087		D
transport	Rho3	15.4310		D
transport	Msb1	14.6941		D
signaling	Cdc42	13.5537		D
signaling	Bem1	10.1558		D

LSMean: Least Square Mean

Table S7. Global paramenters for 29 proteins in Transport module and Signaling module

	$t_{1/2}$	degree	clustering coefficient	eccentricity	betweenness	Participation coefficient	z-score
BEM1	10.16	14	0.27	4	346.74	0.63	-0.26
BEM3	19.00	4	0.17	5	14.23	0.49	2.03
BNI1	21.38	12	0.18	4	306.16	0.00	-0.28
BOI1	23.98	4	1.00	4	0.00	0.28	0.01
BOI2	16.52	6	0.60	4	37.05	0.00	-0.26
BUD6	25.20	10	0.29	4	166.66	0.00	-0.87
CDC24	16.41	13	0.33	4	186.42	0.45	2.95
CDC42	13.55	21	0.17	4	782.91	0.00	-1.5
CLA4	17.74	12	0.21	4	192.70	0.32	-0.64
GIC1	22.21	3	1.00	5	0.00	0.53	0.01
LRG1	49.00	3	0.00	5	61.64	0.00	-0.12
MKK1	23.53	3	0.00	5	26.66	0.00	-0.87
MSB1	14.69	2	0.00	5	1.72	0.45	0.74
MSB3	17.90	7	0.33	4	90.14	0.00	0.97
MSB4	25.32	7	0.33	4	96.46	0.59	0.74
MYO2	16.43	9	0.14	5	214.33	0.48	-0.93
PEA2	92.30	6	0.40	5	79.47	0.41	-0.07
PKC1	29.90	4	0.00	5	54.16	0.00	-0.98
PXL1	22.40	1	0.00	6	0.00	0.00	0.01
RGA1	29.36	8	0.14	4	111.55	0.38	-0.12
RGD1	24.19	4	0.00	5	148.46	0.00	-0.55
RGD2	16.59	2	0.00	5	97.00	0.38	-0.12
RHO1	72.30	10	0.04	5	394.13	0.00	-0.98
RHO3	15.43	4	0.00	5	81.50	0.00	-0.55
ROM2	22.91	2	0.00	5	27.72	0.15	1.34
SMY1	20.27	1	0.00	6	0.00	0.48	1.6
SPA2	30.06	10	0.20	4	281.58	0.44	-1.56
STE20	17.85	15	0.16	4	439.29	0.63	0
YOR304C-A	29.73	2	1.00	5	0.00	0.50	-0.98
average	26.08	6.86	0.24	4.62	146.16	0.26	-0.04
Correlation coefficient between $t_{1/2}$ and global parameters:		-0.10	0.02	0.21	-0.03	-0.11	-0.17
		A	B	C	D	E	F

A: correlation between $t_{1/2}$ and degree
B: correlation between $t_{1/2}$ and clustering coefficient
C: correlation between $t_{1/2}$ and eccentricity
D: correlation between $t_{1/2}$ and betweenness
E: correlation between $t_{1/2}$ and Participation Coefficient
F: correlation between $t_{1/2}$ and Z-score

Table S8. For most of the 29 proteins, there is no significant difference of the dynamics between interaction partners and non-interaction partners

protein name	direct_mean	indirect_mean	self_mean	direct p value	indirect p value
Bem1	35.18579313	20.4200025	20.29053677	0.029284367	0.999453147
Bem3	22.16449378	25.47004966	25.4260303	0.848077688	0.999957955
Bni1	25.17449117	25.54996367	14.31911051	0.148577758	0.128636953
Boi1	20.36943696	26.08663267	29.78392211	0.244261402	0.736717846
Boi2	18.12387658	28.0709584	20.83555692	0.829057016	0.384624999
Bud6	24.77557506	25.50010166	18.2009402	0.430359221	0.360273805
Cdc24	21.68480089	26.86861351	21.43040874	0.998191532	0.534614185
Cdc42	23.41198322	28.45603099	18.05252687	0.539930096	0.233742151
Cla4	24.30578123	25.70635726	23.91960297	0.996351782	0.936990943
Gic1	22.34634008	25.28820336	28.80837161	0.56330568	0.780396886
Lrg1	49.57247335	22.27711449	42.89716174	0.449156949	0.001364365
Mkk1	22.85327422	25.57026714	16.42044772	0.54070119	0.245110205
Msb1	18.9455585	26.12290547	7.637098795	0.224553284	0.008691618
Msb3	42.61289748	21.45390865	13.16625143	1.22873E-06	0.186960233
Msb4	31.15164233	23.99075189	18.59142598	0.099604194	0.512872609
Myo2	13.9622052	27.25109492	7.64310228	0.404214413	0.000541832
Pea2	18.57977452	24.2033472	86.55516366	9.99978E-13	9.99978E-13
Pkc1	50.12688838	23.21575298	25.13566874	0.000153343	0.881134011
Pxl1	23.45519429	25.52291169	15.54061371	0.559010985	0.208813964
Rga1	42.48827801	21.6535067	37.71609318	0.60168499	0.014368333
Rgd1	8.042241793	25.85148207	16.79776579	0.490386237	0.264994085
Rgd2	17.981655	25.83284746	23.03816779	0.678636315	0.833611673
Rho1	23.62373005	23.01751404	67.63079073	9.99978E-13	9.99978E-13
Rho3	11.46697195	27.05533248	6.838391381	0.652504284	0.003111965
Rom2	67.44807956	23.31229875	18.06443312	9.99978E-13	0.506595814
Smy1	8.717449835	26.17674736	12.5571785	0.818679808	0.061952758
Spa2	23.06601882	25.77718193	22.74732693	0.996867955	0.780361927
Ste20	21.35687704	26.7160152	23.29223319	0.90599407	0.758440988
Yor304c-a	18.27848111	25.42256076	22.77475211	0.817038227	0.874000593

Table S9 . $t_{1/2}$ values for 2 proteins in Mitotic Exit module
(equation $Y = A0 + A^* \exp(-\omega * t)$ was used for iFRAP curve fitting, for details see supplementary online material.)

	Kel1	Lte1
curve 1	45.74	44.01
curve 2	85.76	43.59
curve 3	146.20	69.98
curve 4	149.13	37.11
curve 5	83.57	68.72
curve 6	55.93	31.97
curve 7	63.05	46.87
curve 8	80.19	39.01
curve 9	57.39	80.16
curve 10	106.90	36.37

Table S10. $t_{1/2}$ values for 11 proteins in *pea2Δ*
(equation $Y = A0 + A^* \exp(-\omega * t)$ was used for iFRAP curve fitting, for details see supplementary online material.)

	Δpea2 Rga1-GFP	*Δpea2 GFP-Cdc42p*	*Δpea2 Bni1-GFP*	*Δpea2 Pkc1p-GFP*
curve 1	12.78	17.40	14.29	21.92
curve 2	32.83	10.07	13.39	17.83
curve 3	42.38	11.19	16.83	19.96
curve 4	11.95	20.98	12.53	14.15
curve 5	14.33	16.40	27.54	38.32
curve 6	37.17	7.08	20.19	24.49
curve 7	18.70	10.95	30.32	9.49
curve 8	24.15	5.26	16.49	14.89
curve 9	34.15	5.09	10.25	11.18
curve 10	35.92	8.88	10.43	8.11

	Δpea2 GFP-Rho3p	*Δpea2 Yor304c-a-GFP*	*Δpea2 Bud6-GFP*	*Δpea2 Myo2-GFP*
curve 1	23.21	12.66	19.46	17.92
curve 2	13.97	11.39	11.50	19.63
curve 3	18.49	14.03	11.33	11.46
curve 4	8.35	10.56	15.94	15.78
curve 5	18.24	14.04	8.20	27.21
curve 6	16.64	16.83	10.09	31.55
curve 7	17.00	17.47	11.11	46.32
curve 8	32.52	31.40	12.84	8.28
curve 9	4.26	4.49	5.20	23.42
curve 10	40.75	4.82	14.19	19.64

	Δpea2 Spa2-GFP	*Δpea2 Lrg1-GFP*	*Δpea2 GFP-Rho1p*
curve 1	13.30	41.16	59.49
curve 2	10.45	63.31	26.08
curve 3	11.84	24.51	28.66
curve 4	25.05	61.02	43.68
curve 5	18.99	75.17	26.08
curve 6	22.79	31.87	38.04
curve 7	14.15	45.78	37.98
curve 8	16.80	45.50	28.94
curve 9	30.53	56.13	33.64
curve 10	30.66	38.09	33.24
curve 11	6.44	48.35	27.22
curve 12		48.87	22.83
curve 13		40.39	26.68
curve 14			13.94
curve 15			69.61
curve 16			58.15
curve 17			19.13
curve 18			33.39

Table S11. Yeast strains used in this study

Strain	Mat	Relevant genotype (*)	Source
RLY4555	*a*	*pea2∆::KanR BNI1-* GFP*::HIS3*	from this paper
RLY4526	*a*	*pea2Δ::KanR BUD6-* GFP*::HIS3*	from this paper
RLY4528	*a*	*pea2Δ::KanR MYO2-* GFP*::HIS3*	from this paper
RLY4530	*a*	*pea2Δ::KanR SPA2-* GFP*::HIS3*	from this paper
RLY4553	*a*	*pea2Δ::KanR PKC1-* GFP*::HIS3*	from this paper
RLY4851	*a*	*pea2Δ::KanR YOR304C-A-* GFP*::URA3*	from this paper
RLY4852	*a*	*pea2Δ::KanR RGA1-* GFP*::URA3*	from this paper
RLY4853	*a*	*pea2Δ::KanR LRG1-* GFP*::URA3*	from this paper
RLY4531	*a*	*pea2Δ::KanR RHO1::GFP-RHO1-myc6::URA3*	from this paper
RLY4533	*a*	*pea2Δ::KanR RHO3::* GFP*-RHO3-* myc6*::URA3*	from this paper
RLY4535	*a*	*pea2Δ::KanR CDC42::* GFP*-CDC42* -myc6*::URA3*	from this paper
RLY3479	*a*	*BNI1* -GFP*::HIS3*	Huh *et al.* , Nature 2003.
RLY2912	*a*	*CLA4-* GFP*::HIS3*	Huh *et al.* , Nature 2003.
RLY2550	*a*	*LRG1-* GFP*::HIS3*	Huh *et al.* , Nature 2003.
RLY2908	*a*	*GIC1-* GFP*::HIS3*	Huh *et al.* , Nature 2003.
RLY2907	*a*	*BOI2-* GFP*::HIS3*	Huh *et al.* , Nature 2003.
RLY2766	*a*	*BEM1-* GFP*::HIS3*	Huh *et al.* , Nature 2003.
RLY2913	*a*	*MSB4-* GFP*::HIS3*	Huh *et al.* , Nature 2003.
RLY2910	*a*	*BOI1-* GFP*::HIS3*	Huh *et al.* , Nature 2003.
RLY2544	*a*	*RGA1-* GFP*::HIS3*	Huh *et al.* , Nature 2003.
RLY2556	*a*	*RGD2-* GFP*::HIS3*	Huh *et al.* , Nature 2003.
RLY2557	*a*	*RGD1-* GFP*::HIS3*	Huh *et al.* , Nature 2003.
RLY2558	*a*	*BUD6-* GFP*::HIS3*	Huh *et al.* , Nature 2003.
RLY2769	*a*	*PKC1-* GFP*::HIS3*	Huh *et al.* , Nature 2003.
RLY2916	*a*	*STE20-* GFP*::HIS3*	Huh *et al.* , Nature 2003.
RLY2767	*a*	*CDC24-* GFP*::HIS3*	Huh *et al.* , Nature 2003.
RLY2877	*a*	*MYO2-* GFP*::HIS3*	Huh *et al.* , Nature 2003.
RLY2770	*a*	*MSB1-* GFP*::HIS3*	Huh *et al.* , Nature 2003.
RLY3090	*a*	*BEM3-* GFP*::HIS3*	Huh *et al.* , Nature 2003.
RLY3243	*a*	*SMY1-* GFP*::HIS3*	Huh *et al.* , Nature 2003.
RLY3239	*a*	*PXL1-* GFP*::HIS3*	Huh *et al.* , Nature 2003.
RLY3119	*a*	*SPA2-* GFP*::HIS3*	Huh *et al.* , Nature 2003.
RLY4606	*a*	*PEA2-* GFP*::HIS3*	Huh *et al.* , Nature 2003.
RLY4608	*a*	*MKK1-* GFP*::HIS3*	Huh *et al.* , Nature 2003.
RLY4610	*a*	*ROM2-* GFP*::HIS3*	Huh *et al.* , Nature 2003.
RLY4613	*a*	*YOR304C-A-* GFP*::HIS3*	Huh *et al.* , Nature 2003.
RLY4609	*a*	*MSB3-* GFP*::HIS3*	Huh *et al.* , Nature 2003.
RLY3238	*a*	*BEM2-* GFP*::HIS3*	Huh *et al.* , Nature 2003.
RLY2914	*a*	*LTE1-* GFP*::HIS3*	Huh *et al.* , Nature 2003.
RLY2768	*a*	*KEL1-* GFP*::HIS3*	Huh *et al.* , Nature 2003.
RLY3387	*a*	*RHO3::GFP-Rho3-myc6::URA3*	from this paper
RLY3385	*a*	*RHO1::GFP-Rho1-myc6::URA3*	from this paper
RLY2902	*a*	*CDC42::GFP-Cdc42-myc6::URA3*	from this paper
RLY4547	*a*	*SPA2-* mCherryOPT*::URA3 PEA2-* GFP*::HIS3*	from this paper
RLY4548	*a*	*PEA2-mCherryOPT::HIS3 RHO1::* GFP*-RHO1-myc6::URA3*	from this paper

All strains are of S288C background and others with same type of genotype (markers)